



# City Research Online

## City, University of London Institutional Repository

---

**Citation:** Zhang, T., Taylor, R. N., Divall, S. ORCID: 0000-0001-9212-5115, Zheng, G., Sun, J., Stallebrass, S. E. ORCID: 0000-0002-3747-9524 and Goodey, R.J. ORCID: 0000-0002-9166-8393 (2019). Explanation for twin tunnelling-induced surface settlements by changes in soil stiffness on account of stress history. *Tunnelling and Underground Space Technology*, 85, pp. 160-169. doi: 10.1016/j.tust.2018.12.015

This is the accepted version of the paper.

This version of the publication may differ from the final published version.

---

**Permanent repository link:** <https://openaccess.city.ac.uk/id/eprint/21230/>

**Link to published version:** <http://dx.doi.org/10.1016/j.tust.2018.12.015>

**Copyright and reuse:** City Research Online aims to make research outputs of City, University of London available to a wider audience. Copyright and Moral Rights remain with the author(s) and/or copyright holders. URLs from City Research Online may be freely distributed and linked to.

---

City Research Online:

<http://openaccess.city.ac.uk/>

[publications@city.ac.uk](mailto:publications@city.ac.uk)

---

1     **Explanation for Twin Tunnelling-induced Surface Settlements by**  
2             **Changes in Soil Stiffness on Account of Stress History**

3     Tianqi Zhang<sup>1</sup>, R Neil Taylor<sup>2</sup>, Sam Divall<sup>2</sup>, Gang Zheng<sup>1</sup>, Jibin Sun<sup>1</sup> Sarah Elizabeth  
4                             Stallebrass<sup>2</sup>, and Richard James Goodey<sup>2</sup>

5             <sup>1</sup>School of Civil Engineering, Tianjin University, Tianjin 300072, China.

6             <sup>2</sup>School of Engineering and Mathematical Sciences, City, University of London,  
7                             Northampton Square, EC1V 0HB London, UK

8     **Abstract:** In this article, a group of representative centrifuge tests were selected for  
9     numerical modelling to explain the surface settlements induced by sequential twin  
10    tunnelling. Both Modified Cam Clay model (MCC) and Three-Surface Kinematic  
11    Hardening model (3-SKH) were adopted in the simulation, which indicated the use of  
12    3-SKH model conduced to mimicking more closely centrifuge model response. Via  
13    performing more contrastive numerical analyses with 3-SKH model, the influence of  
14    the first tunnel event on the stiffness of the soil around the second tunnel was  
15    quantitatively investigated, whereby the mechanism behind the observed surface  
16    settlements was finally made clear.

17    Keywords: twin tunnelling; Modified Cam Clay model; Three-Surface Kinematic  
18    Hardening model; stiffness of soil

19 **1. INTRODUCTION**

20 Tunnels for mass transit systems are often constructed in pairs to facilitate travel  
21 in opposite directions. This arrangement is well known as twin-tunnelling. For the  
22 purpose of calculating settlements, O'Reilly and New (1982) suggested superposition  
23 of settlement profiles predicted for individual tunnels (Peck, 1969; Mair, 1979; Taylor,  
24 1984). However, this simplified method was first challenged by field observations  
25 (Nyren, 1998; Cording and Hansmire, 1975; Cooper and Chapman, 1998; Cooper *et*  
26 *al.*, 2002; Fagnoli *et al.*, 2015), which showed that the surface settlements, in particular  
27 those generated by the second tunnel, would be potentially underestimated.

28 Chapman *et al.* (2007) performed 1 g physical model tests to investigate the  
29 ground movements subjected to the twin tunnel construction under controlled  
30 laboratory conditions. Greater surface settlements were shown to be generated by the  
31 second tunnel. This suggested that it ought to be the presence of the first tunnel  
32 influencing the behaviour of the second as other uncertainties in field sites can be  
33 excluded in the laboratory tests. Recently, Divall and Goodey (2012) further explored  
34 the twin tunnelling-induced ground movements using geotechnical centrifuge  
35 modelling as this technique guaranteed a correct stress distribution consistent with that  
36 of a prototype. Similarly, a relative increase in surface settlements due to the second  
37 tunnel was also observed. As equal volume loss was imposed for each tunnel, a

38 rationale behind such observations could be a reduced stiffness within certain areas of  
39 soil mass (Divall and Goody, 2015). A further validation for this would be beyond the  
40 capability of the physical model but may be investigated by numerical modelling  
41 (Addenbrook, 1996), which could explore the stress paths around the second tunnel so  
42 as to provide more information on any changes in soil stiffness and therefore a  
43 understanding of the displacements (Divall, 2013).

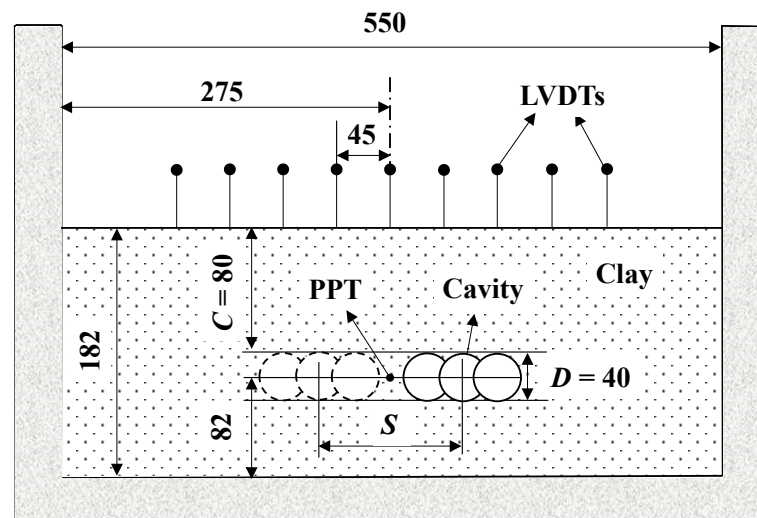
44 In this article, numerical modelling, which was tailored for the above mentioned  
45 centrifuge tests, was conducted with the experimental process carefully replicated, as  
46 far as possible, so as to get an insight into what exactly happened during the tests. Both  
47 a simple, but commonly used Modified Cam Clay (MCC) model (Roscoe and Burland,  
48 1968) and an advanced Three-Surface Kinematic Hardening (3-SKH) model  
49 (Stallebrass, 1990) were adopted in the course of the analyses. The predictive  
50 capabilities of the two models were examined by a comparison against the test data,  
51 making it possible to establish which features of the observed response can be  
52 adequately reproduced by a simple elastoplastic model while others require complex  
53 behaviour of the soil to be replicated. In this way, both the flaws of a MCC model and  
54 the advantages of a 3-SKH model in simulating a twin tunnelling problem were made  
55 clear. More importantly, as the constitutive framework of 3-SKH model was proposed  
56 originally to simulate the effect of previous stress history on subsequent soil behaviour,

57 the changes in soil stiffness around the second tunnel due to the first can be investigated  
58 quantitatively. This provided a chance to explain in fundamental terms the  
59 characteristics of the observed surface settlements in the twin tunnelling centrifuge tests.

## 60 2. CENTRIFUGE TESTS

### 61 2.1 Brief Introduction

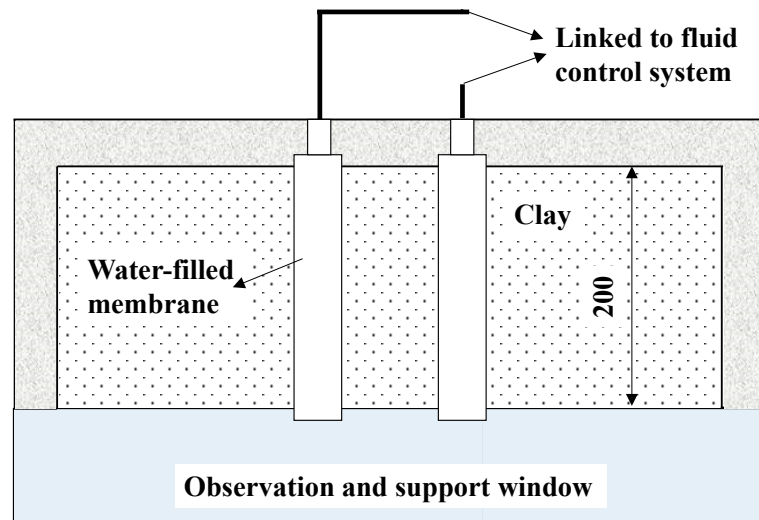
62 Three typical centrifuge tests, performed by [Divall \(2013\)](#) at City, University of  
63 London, were investigated in this article. A generic schematic of the centrifuge models  
64 can be seen in [Fig. 1](#). The tests were in a plane strain configuration, only varying in  
65 tunnel centre to centre spacing (with a spacing  $S$  of  $1.5D$ ,  $3.0D$  and  $4.5D$ , respectively).



66

67

(a) Cross section view

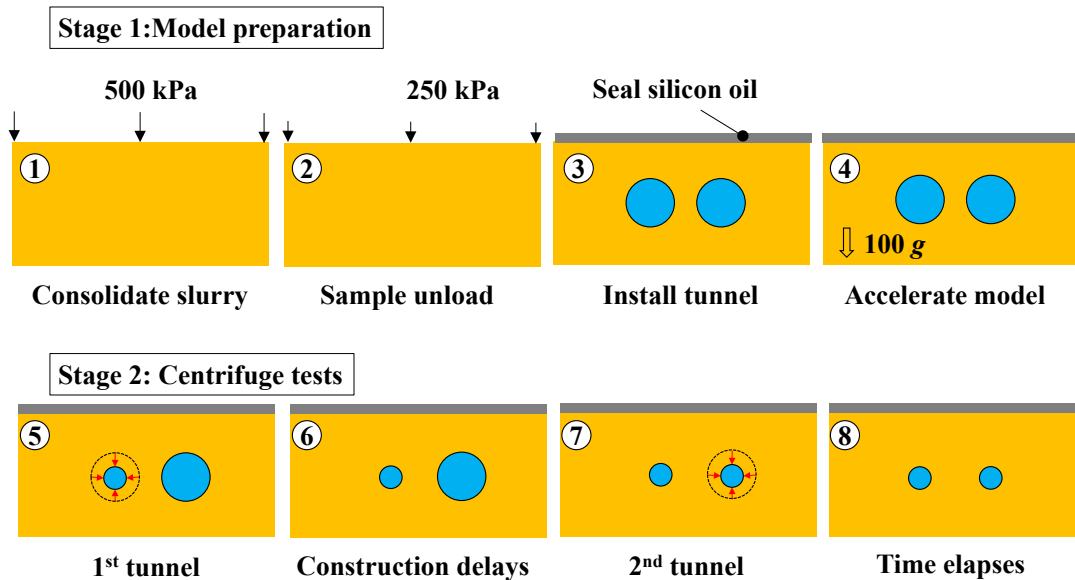


(b) Plan view

Fig. 1 Schematic of plane strain centrifuge models (Unit: mm)

68  
 69  
 70  
 71 Speswhite Kaolin clay slurry was consolidated in the centrifuge strong box to give  
 72 a clay sample of being 550 mm wide, 182 mm high and 200mm thick. Two cylindrical  
 73 cavities were cut in the sample and these would model the twin tunnels. The two cavities  
 74 each had a diameter  $D$  of 40 mm and a cover  $C$  of 80 mm and were supported by water  
 75 within a latex membrane. Volume loss due to tunnelling was simulated by extracting a  
 76 predetermined volume of water from inside the latex membrane via a bishop ram  
 77 equipped in the fluid control system. 9 Linear Variable Differential Transformers  
 78 (LVDTs) were placed symmetrically about the model centre with a uniform spacing of  
 79 45mm to measure the surface settlements. One pore pressure transducer (PPT) was  
 80 installed into the model at the midpoint between the two tunnels to measure the changes  
 81 in pore pressure during the tests.

82 All the tests were carried out on models reduced by a scale factor  $N$  of 100 and  
 83 accelerated to 100 g, following the centrifuge scaling laws (Schofield A,N., 1980). A  
 84 flow chart of the experimental procedure can be seen in Fig. 2.



85  
 86 Fig. 2 Flow chart of experimental procedure

87 The experimental procedure can be divided into two stages:

88 *Stage 1: Model preparation (include 4 steps)*

89 Step 1: Consolidate slurry. The clay slurry with a water content of 120% was  
 90 initially placed inside a rectangular container and consolidated one-dimensionally in a  
 91 hydraulic press to achieve a desired stress history by consolidation to a vertical effective  
 92 stress of 500 kPa.

93 Step 2: Sample unload. The vertical total stress was reduced so that the vertical  
 94 effective stress decreased to 250 kPa after a period of swelling.

95           Step 3: Install tunnel. Once the sample was removed from the consolidation press,  
96 the exposed surface of clay was quickly sealed with silicon oil to prevent evaporation  
97 of water from the sample. Then the front-wall of the strong box was removed to gain  
98 access to the front clay surface, and approximately 4 hours were subsequently left for  
99 boring cavities and installing the tunnel apparatus.

100           Step 4: Accelerate model. Once the model making was completed, the assembled  
101 model was placed on the centrifuge swing, accelerated to 100 g within 4 minutes, and  
102 left running for 24 hours to achieve effective stress equilibrium.

103           *Stage 2: Centrifuge tests (include 4 steps)*

104           Step 5: First tunnel. Water was drained from the first tunnel within 60 seconds  
105 using the fluid control equipment to simulate the first tunnel construction. 7.54 ml of  
106 water was removed from the tunnel apparatus to achieve a volume loss of 3%.

107           Step 6: Construction delays. 3 minutes was left for the centrifuge to run before the  
108 second tunnel event, which represented a construction delay of 3 weeks at prototype  
109 scale according to the centrifuge scaling laws.

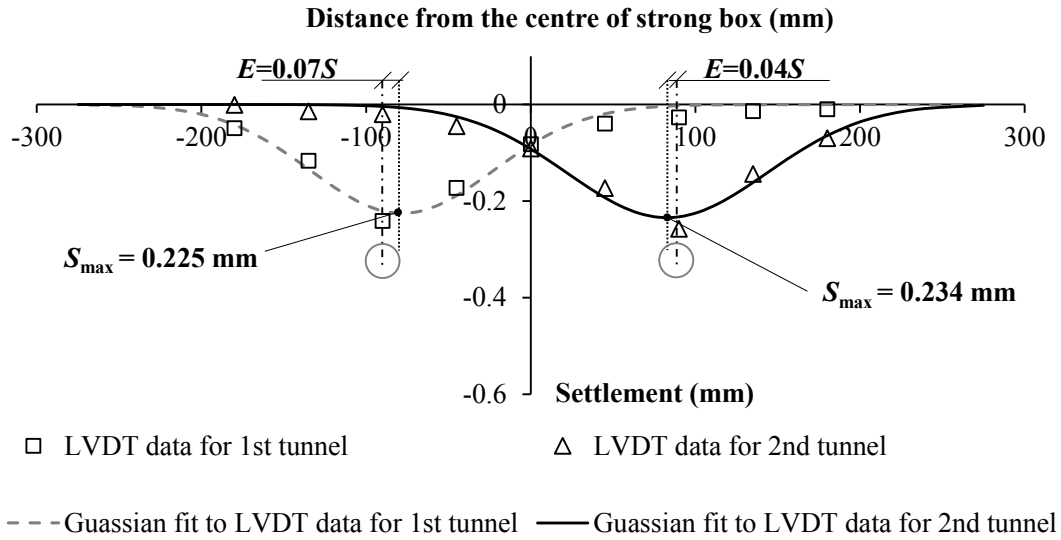
110           Step 7: Second tunnel. Same amount of water was removed from the second tunnel  
111 to simulate the second tunnel construction.

112           Step 8: Time elapses. The centrifuge was left to run for at least an hour post-test  
113 to allow longer term movements to develop.



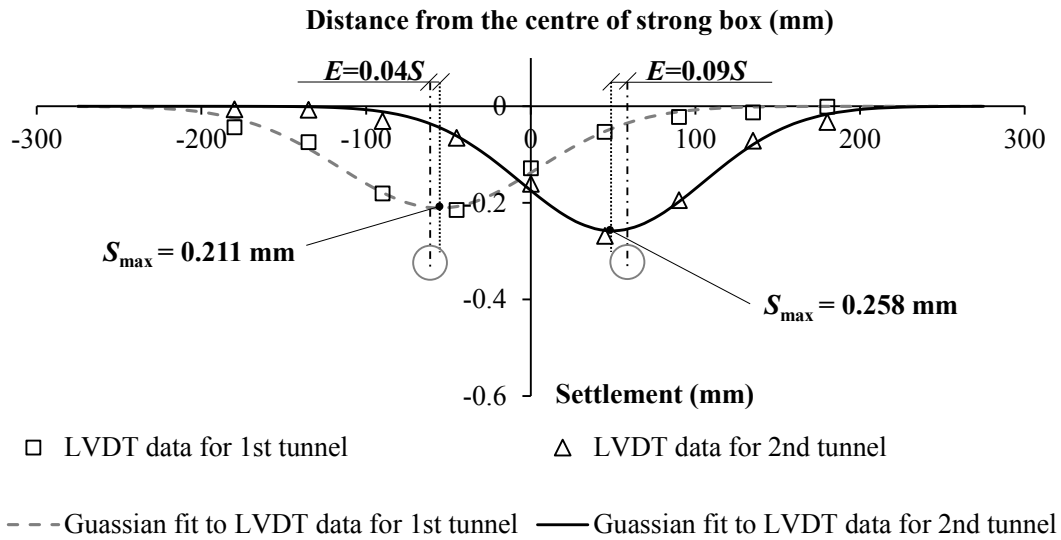
114 **2.2 Characteristics of observed surface settlements**

115 **Fig. 3** shows the observed surface settlements in the three tests.



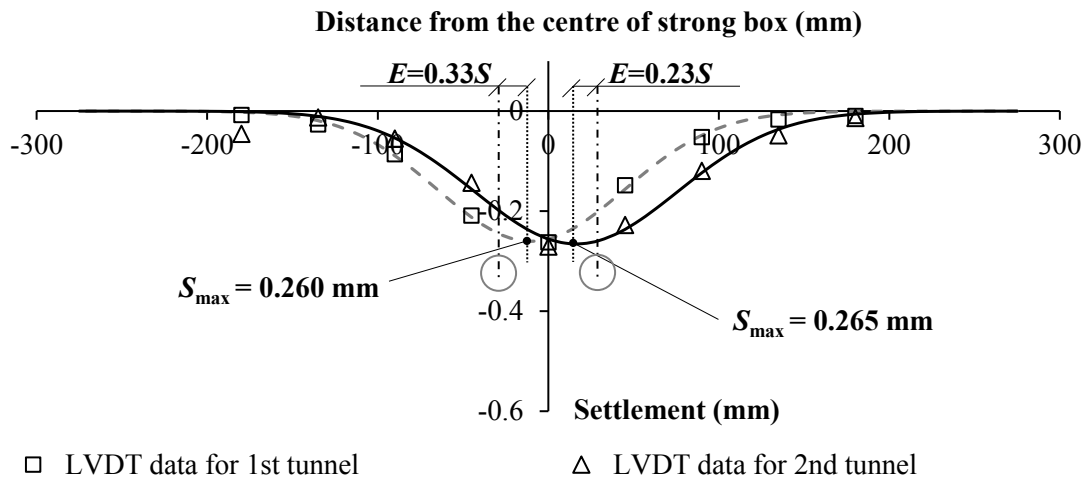
116

117 (a)  $S = 4.5 D$



118

119 (b)  $S = 3.0 D$



□ LVDT data for 1st tunnel                      Δ LVDT data for 2nd tunnel  
 - - - Gaussian fit to LVDT data for 1st tunnel    — Gaussian fit to LVDT data for 2nd tunnel

120

121

(c)  $S = 1.5 D$

122

Fig. 3 Observed surface settlements in three typical tests

123

**Gaussian** curves were fitted separately to the net LVDT data due to each tunnel

124

event. From the fitting results, two basic characteristics of the observed surface

125

settlements can be concluded:

126

*Characteristic 1: Larger  $S_{max}$  due to the second tunnel*

127

As shown in Fig. 3, an increased magnitude of maximum surface settlement  $S_{max}$

128

can be intuitively observed in the second tunnel event when compared to the first.

129

*Characteristic 2: Eccentricity of  $S_{max}$  for the second tunnel*

130

In general, the surface settlement profile should be symmetrical and centred above

131

the tunnel axis for a Greenfield excavation of a single tunnel. However, in Fig. 3, it is

132

clear that the point of  $S_{max}$  for the second tunnel was drawn towards the first tunnel. The

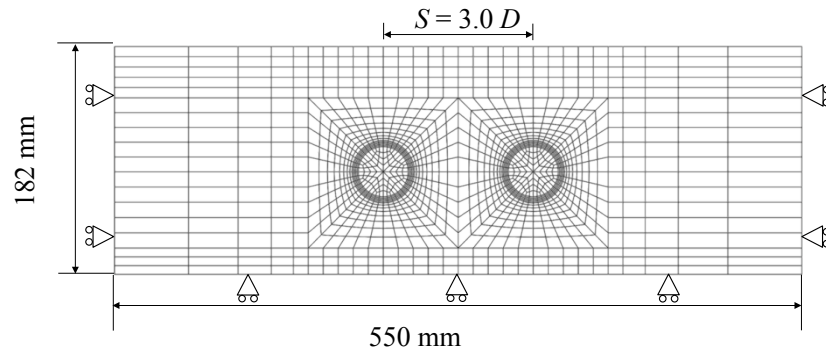
133 offset from the second tunnel axis was termed as the “eccentricity ( $E$ ) of  $S_{\max}$ ”, which  
134 was expressed with the centre-to-centre tunnel spacing  $S$ . It is also interesting to note  
135 another fact from the Gaussian curve fitting that the eccentricity of  $S_{\max}$  also existed in  
136 the first tunnel. This can only be attributed to the influence of the pre-existing second  
137 tunnel prior to the first tunnel event in the centrifuge tests.

138 In fact, characteristic 1 and characteristic 2 has been well recognised in previous  
139 numerical studies (Addenbrooke and Potts, 2001) and physical model tests (Chapman  
140 *et al*, 2007). They were usually considered as a consequence of the additional  
141 subsurface movements in the soil pillars between tunnels (or similarly the “overlapping  
142 zone” proposed by Hunt, 2005) caused by the second excavation in a sequential twin-  
143 tunnelling process. However, the mechanism by which the additional subsurface  
144 movements developed remained unclear. In this sense, detailed numerical modelling  
145 may be helpful, as it can provide a clear insight into the mechanism for the development  
146 of ground movements from a twin-tunnelling type operation.

### 147 **3. NUMERICAL MODELS**

148 Numerical analyses were carried out using commercial finite element software  
149 ABAQUS (version 6.14). A typical schematic drawing of the numerical model is shown  
150 in Fig. 4. The two-dimensional plane-strain model represented a complete section of  
151 the physical model (cf. Fig. 1). Roller boundaries were imposed on the both sides and

152 the base of the model to consider the well-greased condition on them in the centrifuge  
153 tests.



154

155 Fig. 4 Schematic of the numerical model ( $S = 3.0 D$  is shown as an example)

### 156 3.1 Simulation procedure

157 In order to realistically reproduce the load history, the simulation began from  
158 model preparation in analogy with the experimental procedure mentioned before, which  
159 includes 8 steps in total:

160 Step 1: Initial state ( $K_0$  consolidation): The model was initiated by normally  
161 consolidated state. The effective vertical stress was set to 500 kPa and constant with  
162 depth; A  $K_0 = 1 - \sin \phi'$  stress condition was adopted in equilibrium with applied  
163 surcharge of 500 kPa (cf. Fig. 5(a)).

164 Step 2 (One-dimensional swelling): The surcharge was reduced to 250 kPa, while  
165 the pore pressure of the entire model was kept zero, which corresponds to a fully  
166 consolidated process (cf. Fig. 5(b)).

167 Step 3 (Installing tunnels): At the very beginning of step 3, the surcharge was

168 deactivated, meanwhile, a -250 kPa pore pressure was imposed on all nodes of the  
169 model to achieve the same effective stress state as the one at the end of previous step;  
170 Subsequently, the soil in the two cavities was removed, and a total period of 4 hours  
171 was given for this step in accordance with the model making process (cf. Fig. 5(c)).

172 Step 4 (Consolidation in flight): Elastic water elements, with a density of 1000  
173 kg/m<sup>3</sup>, bulk modulus  $K_w$  of 2180 MPa as well as tiny shear modulus  $G_w$ , were activated  
174 in the cavities at the beginning of step 4. These water elements were predefined but  
175 deactivated in the previous three steps, which share the same nodes with the removed  
176 soil elements in step 3 (These water elements were general solid elements without the  
177 degree of pore pressure, therefore, there is no drainage from these water elements to the  
178 surrounding soil elements). Then the acceleration of gravity was increased to 100 *g*  
179 linearly in 4 minutes, followed by a sufficiently long time given for full consolidation.  
180 From this step, the bottom of the model was set completely permeable due to the  
181 drainage grooves there (cf. Fig. 5(d)).

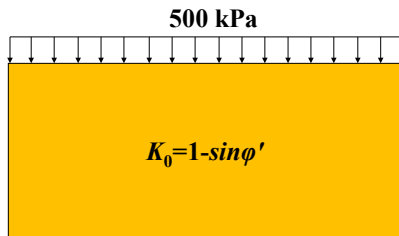
182 Step 5 (First tunnel): “Water” elements inside the first tunnel were removed,  
183 meanwhile, a relatively small support pressure with a fixed gradient of 981 kPa/m along  
184 the depth was applied to the tunnel boundary to achieve a 3% volume loss within the  
185 same time period as in tests (60 seconds). (cf. Fig. 5(e)).

186 Step 6 (Consolidation after first tunnel): The “Water” elements were reactivated

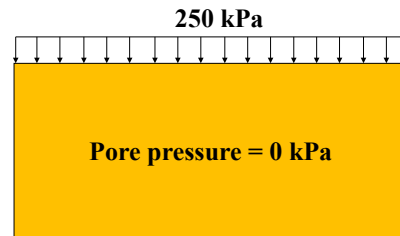
187 inside the first tunnel at the beginning of step 6, followed by a time period of 180  
 188 seconds as a pause to represent a delay before the construction of the second tunnel. It  
 189 should be noted that the “water” elements reactivated in this step were set free of gravity,  
 190 which were employed only to undertake the unbalance force generated in the  
 191 subsequent steps because all loads defined in the previous steps would be inherited in  
 192 ABAQUS by default if without additional definitions (cf. Fig. 5(f)).

193 Step 7 (Second tunnel): Operations taken in step 5 for the first tunnel were repeated  
 194 for the second (cf. Fig. 5(g)).

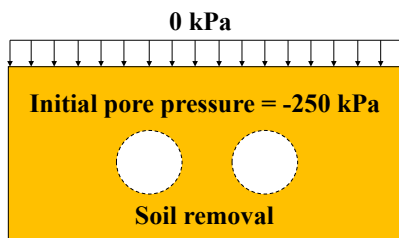
195 Step 8 (Consolidation after second tunnel): Operations taken in step 6 for the first  
 196 tunnel were repeated for the second (cf. Fig. 5(h)).



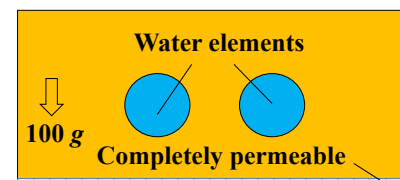
197  
 198 (a)  $K_0$  Consolidation



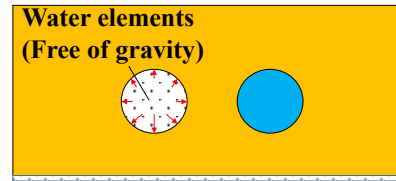
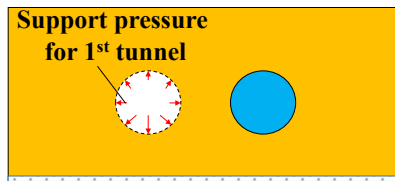
(b) One-dimensional swelling



199  
 200 (c) Installing tunnels



(d) Consolidation in flight

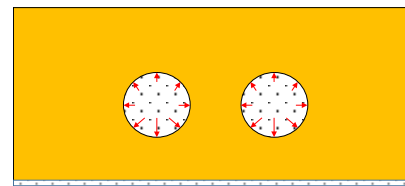
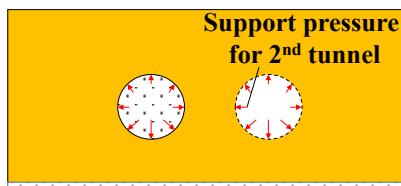


201

202

(e) First tunnel

(f) Consolidation after first tunnel



203

204

(g) Second tunnel

(h) Consolidation after second tunnel

205

Fig.5 Simulation procedure for centrifuge tests (not scaled)

206

### 3.2 Constitutive models

207

Both Modified Cam Clay (MCC) model and Three-Surface Kinematic Hardening

208

(3-SKH) model were adopted in the numerical analyses. The 3-SKH model can be

209

considered as an extension of MCC model, which introduced two additional surfaces,

210

i.e., the yield surface (YS) and the history surface (HS) inside a MCC critical state

211

bounding surface (BS), as shown in Fig. 6. This makes it possible to simulate the

212

behaviour of soil over a wide range of strain levels as well as with changes of stress

213

path direction (Stallebrass, 1990).

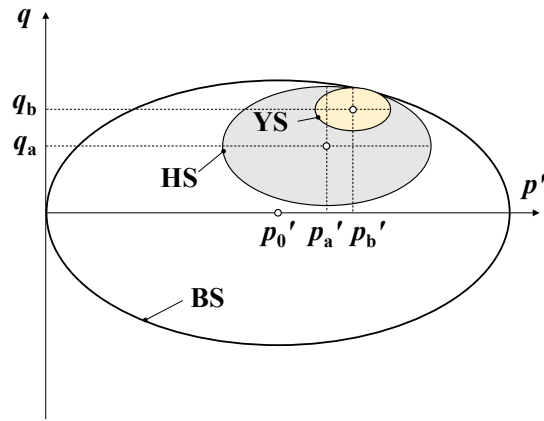


Fig. 6 Sketch of 3-SKH model in  $p'$ - $q$  plane

214

215

216 The 3-SKH model was implemented using a user-defined material subroutine  
 217 (UMAT), which was reprogrammed in FORTRAN language, following the original  
 218 version used in CRISP by Stallebrass (1990) as well as the C++ version used in  
 219 TOCHNOG by Masin (2004).

220 The soil parameters of Speswhite kaolin clay for both MCC and 3-SKH model  
 221 have been well established after many calibration works by researchers at City,  
 222 University of London, as shown in table 1.

223 Table 1 Soil parameters for both MCC and 3-SKH model

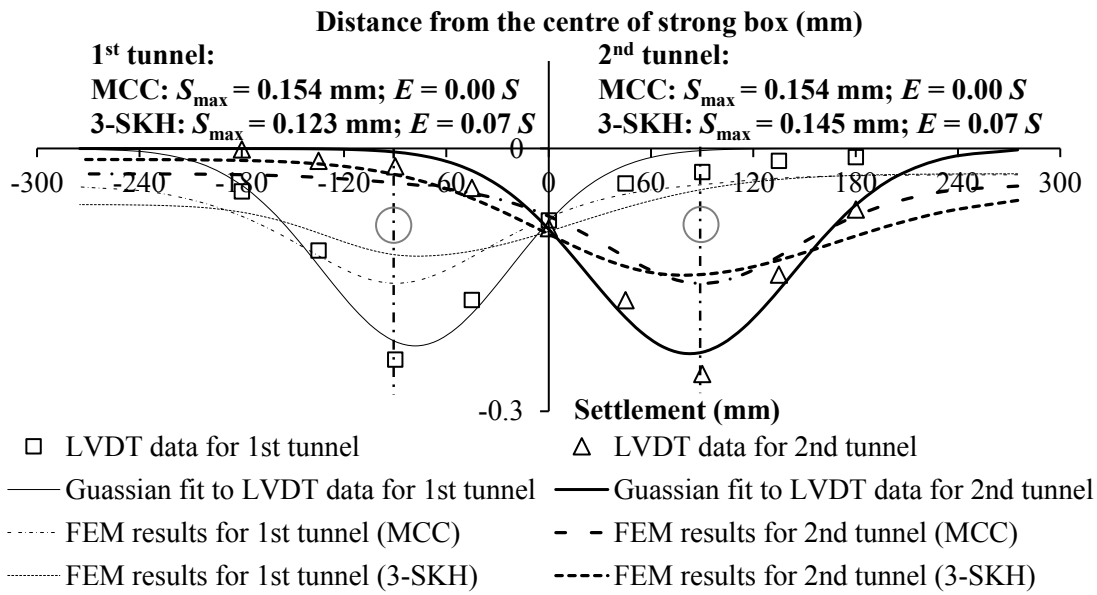
MCC model (Morrison,1994)	$M$	$\lambda$	$\kappa$	$e_{cs}$	$\nu$				$k_v$	$k_h$
									mm/	mm/s
									s	
	0.8	0.18	0.03	1.97	0.3				4.7e-	1.37e
	9		5						7	-6
3-SKH model (Stallebrass, 1990;Viggiani,1992 )	$M$	$\lambda^*$	$\kappa^*$	$e_{cs}$	$A$	$T$	$S$	$\psi$	$k_v$	$k_h$
					kPa				mm/	mm/s
									s	
	0.8	0.07	0.00	1.99	196	0.2	0.0	2.	4.7e-	1.37e
	9	3	5	4	4	5	8	5	7	-6



#### 224 4. VALIDATION OF NUMERICAL MODELS

225 Fig. 7 shows the computed and measured surface settlements. In general, both  
226 *MCC model and 3-SKH predicted wider and shallower settlement troughs when*  
227 *compared to the test data. Predictions closer to the test data might be obtained by*  
228 adjusting the parameters of the model. However, this is not undertaken in this study  
229 since the engineering properties of the used Speswhite kaolin clay have been well  
230 established due to the continuous input into the calibration (e.g., Stallebrass and Taylor,  
231 *1997; Grant, 1998; Masin, 2004; Bilotta and Stallebrass, 2009*).

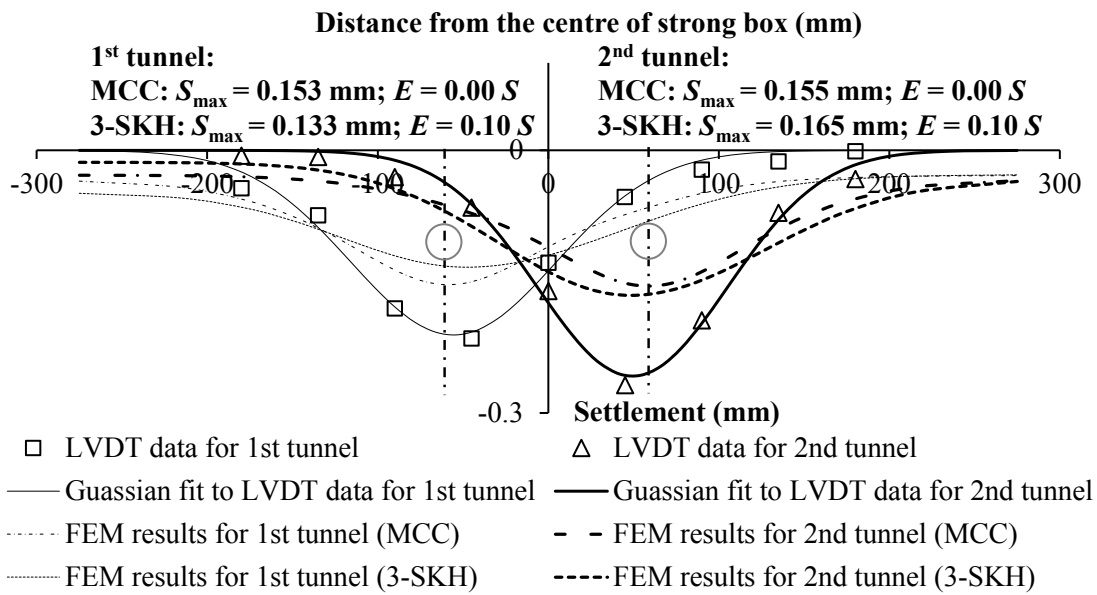
232 It is clear to see that the 3-SKH model was capable of soundly reproducing the  
233 *two basic characteristics (Larger  $S_{max}$  and eccentricity of  $S_{max}$  in the second tunnel event)*  
234 *of the observed surface settlements in the centrifuge tests, whereas MCC model failed*  
235 *to provide those only except for the case with  $S = 1.5 D$ , which implied that the MCC*  
236 model might underestimate the interaction between the two tunnels.



237

238

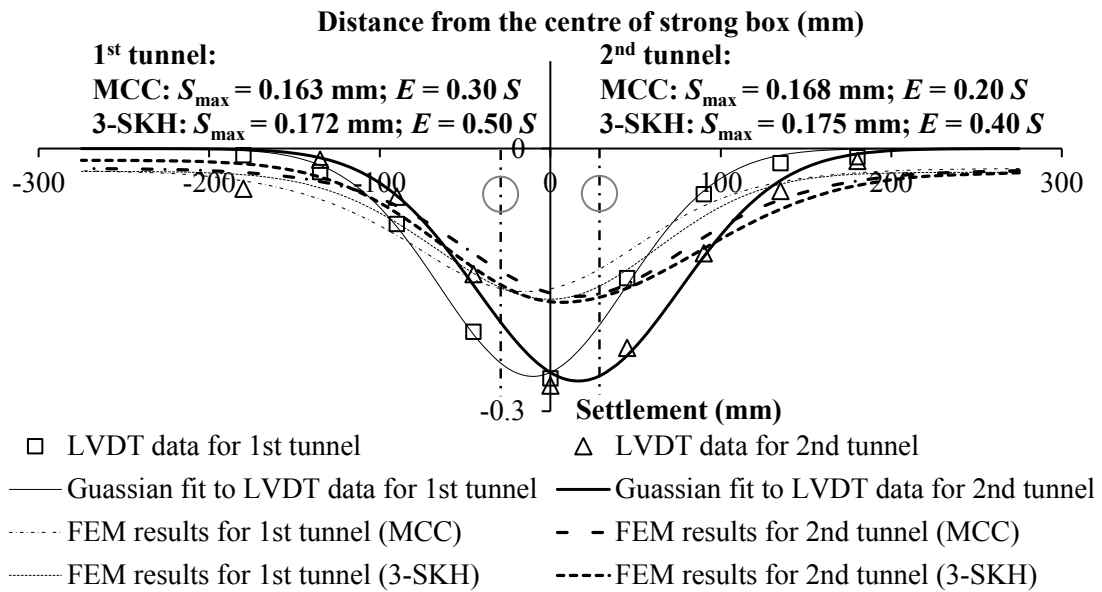
(a)  $S = 4.5 D$



239

240

(b)  $S = 3.0 D$

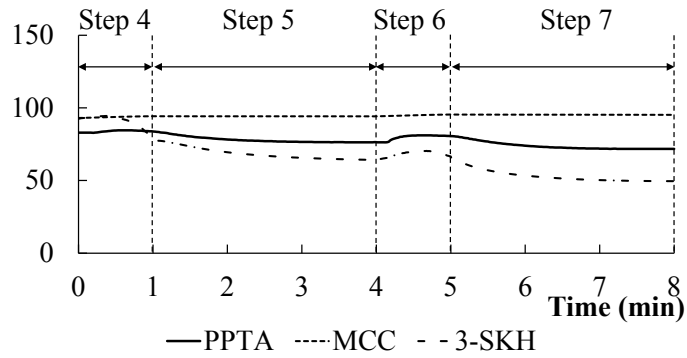


(c)  $S = 1.5 D$

Fig. 7 Comparison of computed and measured surface settlements

Leaving aside the two basic characteristics mentioned above, it is interesting to note that in terms of magnitude of  $S_{\max}$  and width of settlement trough, MCC model seemed better for the prediction of the first tunnel event for the case with  $S = 3.0 D$  and  $S = 4.5 D$ . To further examine the performance of both MCC model and 3-SKH model, comparison was also made between the computed and measured pore pressure changes at the midpoint between the two tunnels (cf. PPT in Fig. 1), as shown in Fig. 8 (PPT was absent in the test with  $S = 1.5 D$ ). The PPT data in the tests with  $S = 3.0 D$  and  $S = 4.5 D$  showed similar regularity, which was seen to rise at the start of each tunnel event as a result of the arching effect (Kim et al, 1998; Lee, 2006), and then to drop before being stabilised due to consolidation. Basically, the changes in pore pressures predicted

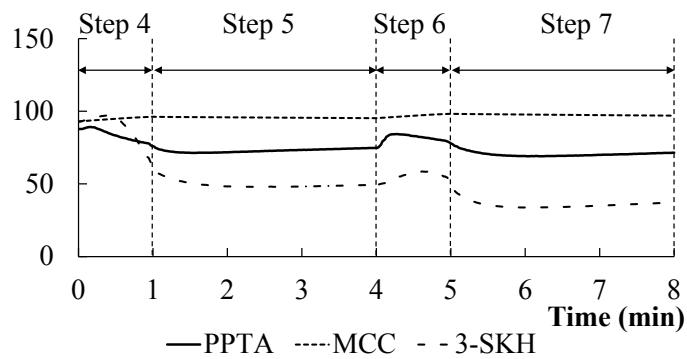
254 by the 3-SKH model were very close to the observed PPT response as described above,  
 255 while the results predicted by MCC model seemed quite imperceptible.



256

257

(a)  $S = 4.5 D$



258

259

(b)  $S = 3.0 D$

260

Fig.8 Comparison of predicted and measured pore pressures

261

As greater changes in PPT readings may be relevant to more significant changes

262

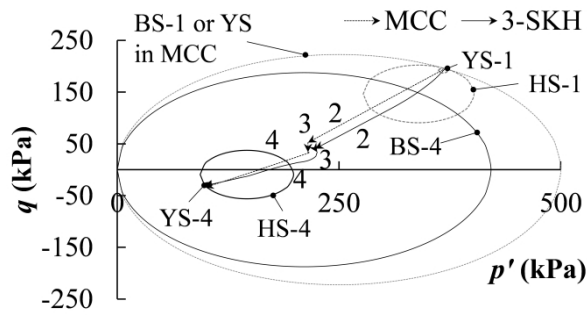
in effective stresses, the stress path at the same position predicted by both the MCC

263

model and the 3-SKH model were also compared, as shown in Fig. 9. Considering the

264

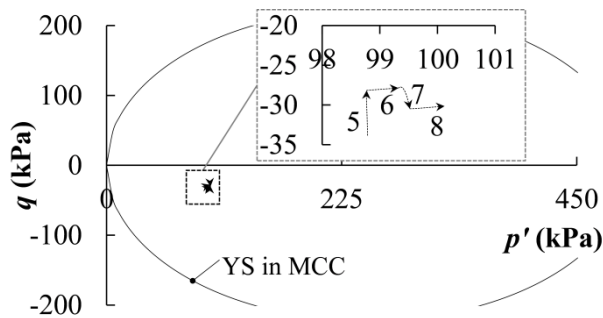
similar regularity, only the stress path in the test with  $S = 3.0 D$  is plotted.



265

266

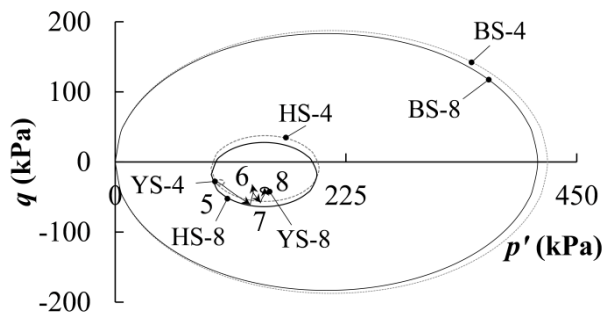
(a) Stress path from step 2 to 4 (both MCC and 3-SKH)



267

268

(b) Stress path from step 5 to 8 (MCC)



269

270

(c) Stress path from step 5 to 8 (3-SKH)

271

Fig. 9 Comparison of effective stress path predicted by MCC and 3-SKH model

272

The comparison began with the model preparation (step 2~4). As can be seen in

273

Fig. 9(a), the two models work under different frameworks. The MCC model computed

274

only elastic strains with a constant stiffness in a fixed yield surface (YS) during

275 unloading; while the 3-SKH model allowed plastic strains to develop inside a shrinking  
276 boundary surface (BS-1 shrunk to BS-4 at the end of step 4) in line with an increasing  
277 void ratio during swelling, and stiffness decrease due to the moving of both history  
278 surface (HS-1 to HS-4) and yield surface (YS-1 to YS-4). In general, the MCC model  
279 and 3-SKH model predicted similar stress path and almost the same stress state at the  
280 end of step 4, which means the MCC model may be satisfactory in providing good  
281 predictions for a monotonic unloading event.

282       Once the test began (step 5~8), the two models started to show distinct predictions  
283 for stress path (cf. Fig. 9(b) and Fig. 9(c)). The MCC model computed quite  
284 imperceptible stress variations compared to the 3-SKH model. This was due to the  
285 elastic assumption for the over consolidated soil around the excavated tunnel, which  
286 may lead to a very gentle change in effective stress at the monitoring point under a 3%  
287 volume loss. By contrast, the 3-SKH model could take the stress history into account,  
288 a much higher stiffness of soil was invoked due to a sudden change in the stress path  
289 direction (see the changes in stress path direction in step 4~8). This ensured a significant  
290 change in effective stress, and hence a comparable magnitude of changes in pore  
291 pressure as observed in the tests.

292       Therefore, in the simulation for a twin-tunnelling event, the MCC model may seem  
293 workable in predicting the surface settlements caused by the first tunnel, however,

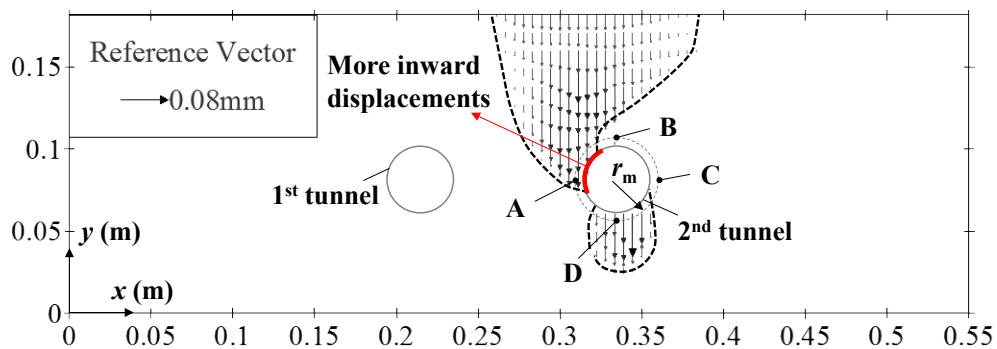
294 would compute a less altered stress field. This may result in a significant  
295 underestimation of the impact of a foregoing tunnel excavation on the surrounding soil,  
296 and hence on the behaviour of the subsequent tunnel. By contrast, due to the superior  
297 performance in modelling the non-linearity of soil stiffness dependent on stress history  
298 in a multi-stage analysis, the predictions obtained using 3-SKH model for both surface  
299 settlements and pore pressure changes were very close to the test data. As a  
300 consequence, only the 3-SKH model is used in the following analyses to explain the  
301 observed surface settlements in the centrifuge tests.

## 302 **5. EXPLANATION FOR OBSERVED SURFACE SETTLEMENTS IN** 303 **CENTRIFUGE TESTS**

304 As mentioned above, two basic characteristics (Larger  $S_{\max}$  and eccentricity of  $S_{\max}$   
305 in the second tunnel event) can be concluded from the observed surface settlements in  
306 the centrifuge tests, which were both well reproduced by numerical simulation with the  
307 3-SKH model.

308 In this section, two cases were simulated using the 3-SKH model for a comparison  
309 of predictions with attempts made to explain the observed surface settlements. In Case  
310 1 the analysis followed the same sequence of events as the centrifuge test with  $S = 3.0$   
311  $D$ , for which both the procedures and the results of the simulation has been detailed in  
312 previous sections. In contrast, case 2 refers to a virtual event, in which the only

313 difference from case 1 was that the volume loss in the first tunnel was set to 0% i.e. no  
 314 unloading. Therefore, case 2 can be considered as an idealised case exclusive of the  
 315 disturbance of the first tunnel to the soil prior to the second tunnel event. The results,  
 316 obtained by subtracting the vertical displacements individually caused by the second  
 317 tunnel in case 2 from the vertical displacements individually caused by the second  
 318 tunnel in case 1, were termed as “additional settlements”, which can be seen in Fig. 10  
 319 (Upheavals have been filtered out so as to clearly show the settlement zone).



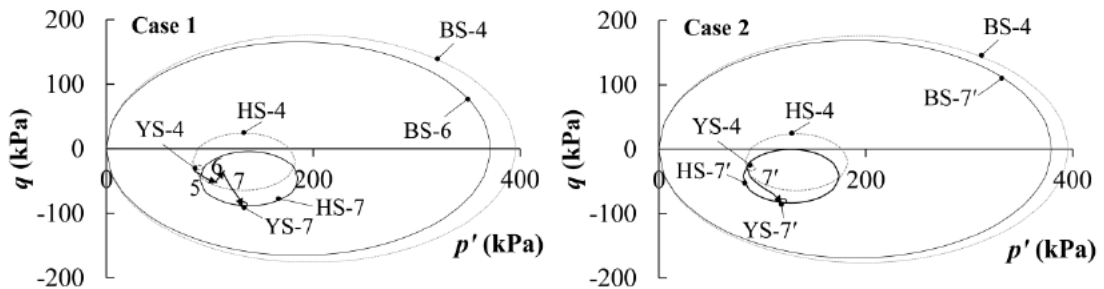
320  
 321 Fig. 10 Computed “additional settlements” due to 2<sup>nd</sup> tunnel

322 As illustrated in Fig. 10, “additional settlements” mainly arose on the left hand  
 323 side (adjacent to the first tunnel) of the region above the second tunnel. With such a  
 324 profile of “additional settlements”, it is not difficult to understand both the increase in  
 325 the magnitude of  $S_{\max}$  and the eccentricity of  $S_{\max}$  due to the second tunnel in case 1.  
 326 Actually, this “additional settlement” profile was found stemming from the more  
 327 inward displacements at the second tunnel springline closer to the first tunnel in case 1.  
 328 Considering that the contraction mode of tunnel during excavation may rely on the

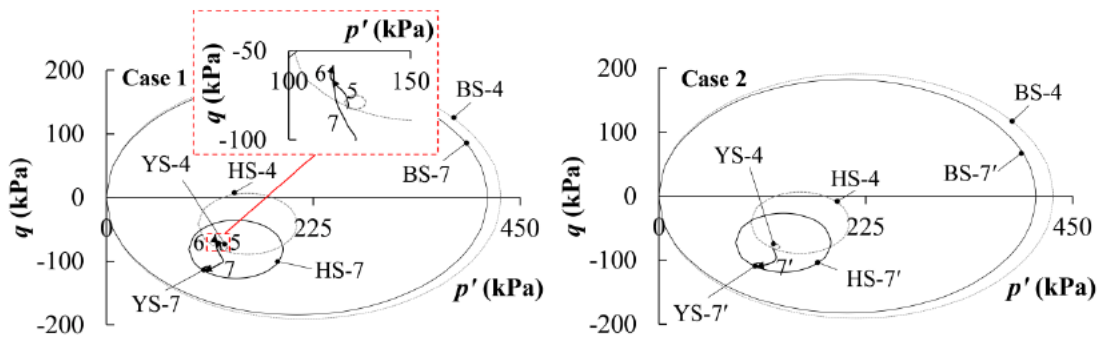


329 stiffness distribution of soil that surrounds the tunnel, four points in the vicinity of the  
 330 second tunnel (point A and C at tunnel springline, B at crown and D at invert) with a  
 331 distance  $r_m$  of  $0.625D$  from the tunnel centre were chosen to compare the stress path  
 332 dependent stiffness of soil during the construction of the second tunnel in both case 1  
 333 and case 2.

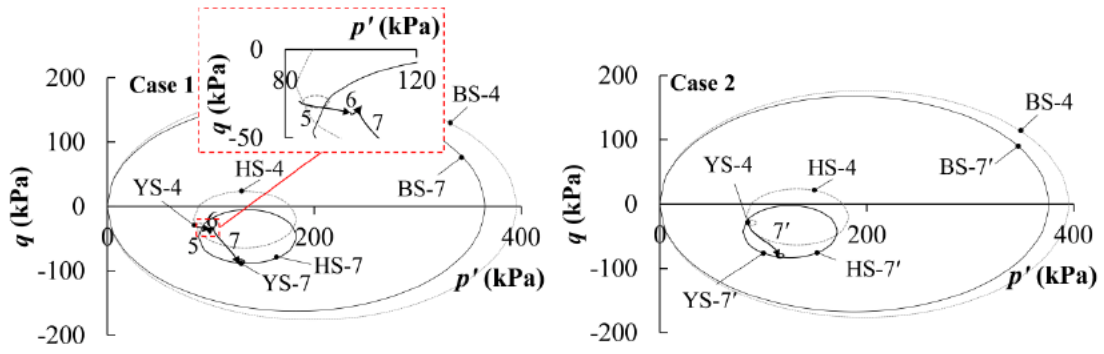
334 Fig. 11 demonstrates the stress paths during the construction of the two tunnels at  
 335 the four points in both case 1 and case 2. Stress path 5, 6, 7 corresponded to step 5, 6  
 336 and 7 in case 1, respectively; while stress path 7' referred to step 7 in case 2 (In case  
 337 2, the stress paths in step 5 and 6 were omitted since there were no changes in the  
 338 effective stress due to the zero volume loss in the first tunnel event).



340 (a) Point A



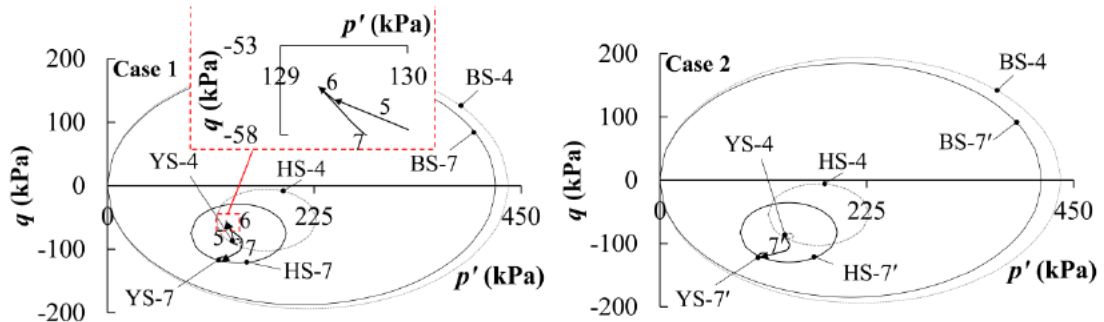
341 (b) Point B



343

344

(c) Point C



345

346

(d) Point D

347 Fig. 11 Comparison of stress paths at four typical points in both case 1 and case

348

2

349 During the construction of the second tunnel (step 7), the soil at the springline of  
 350 the second tunnel (points A and C) was found to be subjected to a compression path  
 351 (cf. stress path 7 and 7' in Fig. 11(a) and Fig. 11(c)), whereas the soil at both the crown  
 352 and invert of the second tunnel (Point B and D) followed an extension path (cf. stress  
 353 path 7 and 7' in Fig. 11(b) and Fig. 11(d)). Meanwhile, from the configuration of the  
 354 kinematic surfaces at the end of step 7, all the history surfaces in the plotted figures  
 355 were shown dragged down (HS-4 to HS-7) following an increase in deviatoric stress  $q$

356 (absolute value), which meant the conjugate point of the stress point on the history  
357 surfaces in stress path 7 (or 7') were located at the bottom half of the surfaces.

358 In case 1, due to the first tunnel, the stress history at point A and C prior to the  
359 second tunnel (stress path 5 and 6) mainly experienced an increase in deviatoric stress  
360  $q$ , which may shorten the distance from the stress point to its conjugate point on the  
361 history surface in the following stress path (stress path 7); while the stress history (stress  
362 path 5 and 6) at point B and D exhibited a decrease in deviatoric stress  $q$ , which may  
363 separate the stress point from its conjugate point on the history surface in the  
364 forthcoming stress path. According to the hardening rule of the 3-SKH model, the  
365 stiffness of soil at a yielded state is relevant to the distance between the stress point and  
366 its conjugate point on the history surface, generally, a larger distance contributes to a  
367 higher stiffness. Therefore, in the second tunnel, different responses of soil stiffness at  
368 the four points would be expected for the two cases, which can be seen in Fig. 12.

369 Following Atkinson *et al.*(1990) and Stallebrass (1990), the notation  $G_c'$  was  
370 adopted in this paper to define the tangential shear modulus, which was obtained by

$$371 \quad G_c' = \frac{1}{3} \left| \frac{dq}{d\varepsilon_s} \right| \quad (1)$$

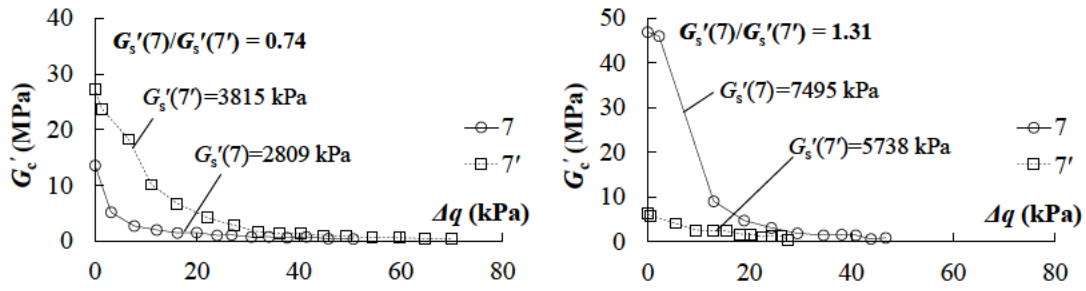
372 Where  $\varepsilon_s$  is shear strain and defined as

$$373 \quad \varepsilon_s = \sqrt{\frac{2}{9} \left\{ (\varepsilon_x - \varepsilon_y)^2 + (\varepsilon_y - \varepsilon_z)^2 + (\varepsilon_x - \varepsilon_z)^2 + 6(\varepsilon_{xy}^2 + \varepsilon_{xz}^2 + \varepsilon_{yz}^2) \right\}} \quad (2)$$

374 To explain the greater volume loss into the second tunnel, Addenbrooke and Potts  
375 (2001) clarified that the excavation of the first tunnel would reduce the stiffness of the  
376 soil in which the second tunnel was then excavated. However, from Fig. 12, it is clear  
377 to see that the response of soil stiffness around the second tunnel was not consistently  
378 softening due to the excavation of the first tunnel. Actually, the response was found to  
379 be highly dependent on the relative changes of the stress path in the two tunnel events.  
380 From the comparison of  $G_c'$  in case 1 and case 2, due to the first tunnel, the soil at the  
381 springline of the second tunnel (point A and C) softened, while the soil at both tunnel  
382 crown and invert hardened. The effect of recent stress history on shear stiffness  
383 decreased as the soil is loaded and vanished with the increase of deviatoric stress  $q$ . It  
384 is the different shear stiffness at the beginning of the second tunnel event which is most  
385 significant. To quantify the softening of soil at point A and C, as well as the hardening  
386 of soil at point B and D due to the first tunnel, the secant shear modulus with a notation  
387 of  $G_s'$  was used in this paper, which was denoted as

388 
$$G_s' = \left| \frac{\Delta q}{\Delta \varepsilon_s} \right| \quad (3)$$

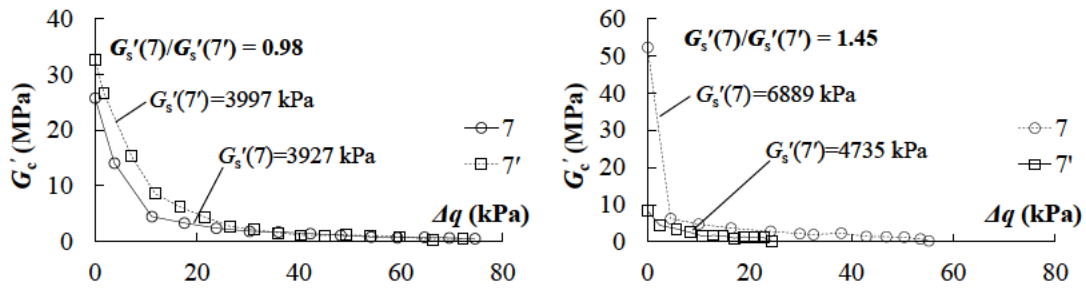
389 Where  $\Delta q$  and  $\Delta \varepsilon_s$  were the change in deviatoric stress and shear strain during tunnel  
390 construction, respectively.



391

(a) Point A

(b) Point B



393

(c) Point C

(d) Point D

395

Fig. 12 Comparison of soil stiffness during step 7 in both case 1 and case 2

396

From the comparison of  $G'_s$  in case 1 and case 2, the softening effect on soil at

397

point A due to the first tunnel was found more significant than that at point C. This was

398

because point A was closer to the first tunnel and may suffer from stronger disturbance.

399

In view of this, as the tunnels were supported by water in the tests, the reduction of the

400

support pressure all around the cavity during tunnelling should be the same. Hence,

401

under the same volume loss (3%), the soil in the region near point B was expected to

402

displace more towards the second tunnel as it was much softer than other regions, and

403

accordingly more settlements would be induced in the soil pillars between the two

404

tunnels, by which the observed surface settlements can be explained.

## 405 6. CONCLUSIONS

406 This study investigated the ground surface settlements induced by sequential twin  
407 tunnelling in over consolidated clay. Credible centrifuge tests were presented first to  
408 show the two basic characteristics of the surface settlements due to a twin-tunnelling  
409 type operation, which were then investigated in detail through the use of both the  
410 Modified Cam Clay model (MCC) and the Three-Surface Kinematic Hardening Model  
411 (3-SKH) in the numerical simulation.

412 The computations using the MCC model could not reproduce the two key  
413 characteristics of the observed surface settlements in the centrifuge tests. Through a  
414 further comparison of the prediction with the pore pressure transducer (PPT) data, the  
415 main reason for the poor performance of the MCC model was addressed. It was  
416 demonstrated that the assumption of elastic response inside the yield surface may under  
417 predict the variations in soil stress around the tunnels, and hence underestimate the  
418 interaction between the two tunnels. By contrast, the 3-SKH model would invoke a high  
419 stiffness if a sudden change in stress path direction was detected in a multi-staged  
420 simulation, which guaranteed considerable changes in soil stress during the  
421 construction of the two tunnels, highlighting the importance of improving the  
422 predictions with the effects of previous stress history on the subsequent stiffness of soil  
423 to be modelled.

424 Under the theoretical framework of the 3-SKH model, the two characteristics of  
425 the observed surface settlements can be successfully explained. Numerical results  
426 indicated that the first tunnel may change the stiffness of the soil around the second  
427 tunnel, which was found associated with the relative changes of stress path in the two  
428 tunnel events. Due to the first tunnel, it was demonstrated that the soil at the springline  
429 of the second tunnel was softened, whereas the soil at both the crown and invert was  
430 hardened. In particular, the softening of soil at the springline adjacent to the first tunnel  
431 was most significant. This may cause an asymmetrical contraction of the second tunnel  
432 during excavation with more inward displacements observed on the softer side, and  
433 more settlements would be induced in the soil pillar between the two tunnels, which  
434 resulted in an increase in the magnitude of  $S_{\max}$  and an eccentricity of  $S_{\max}$  observed in  
435 the second tunnel event.

#### 436 **ACKNOWLEDGEMENTS**

437 The authors would like to acknowledge the financial support from the National  
438 Key R&D Program of China (Grant No. 2017YFC0805407), the National Natural  
439 Science Foundation of China (Grant No. 41630641), the National Natural Science  
440 Foundation of China (Grant No. 51808387), and the National Key R&D Program of  
441 China (Grant No. 2016YFC0802008).

#### **REFERENCES**

Addenbrooke, T.I., 1996. Numerical analysis of tunnelling in stiff clay. Ph.D. thesis, University of London.

Addenbrooke T. and Potts D.M. (2001). Twin tunnel interaction: surface and subsurface effects. *International Journal of Geomechanics* 1(2): 249-271.

Atkinson, J. H., Richardson, D. and Stallebrass, S. E. (1990). Effect of recent stress history on the stiffness of overconsolidated soil. *Géotechnique*. 40(4): 531-40.

Bilotta E. and Stallebrass S.E. (2009). Prediction of stresses and strains around model tunnels with adjacent embedded walls in overconsolidated clay. *Computers and Geotechnics*. 36: 1049-57.

Chapman D.N., Ahn S.K., Hunt D.V.L. (2007). Investigating ground movements caused by the construction of multiple tunnels in soft ground using laboratory model tests. *Canadian Geotechnical Journal*. 44:631-643.

Cooper M.L. and Chapman D.N. (1998). "Movements of the Piccadilly Line tunnels caused by the new Heathrow Express tunnels". *Proc. of the World Tunnel Congress' 98 on tunnels and metropolises, Sao Paulo, Brazil*, pp. 294-254. Balkema.

Cooper, M.L., Chapman, D.N., Roger, C.D.F., Chan, A.H.C., 2002. Movements of the Piccadilly Line tunnels due to Heathrow Express construction. *Géotechnique* 52 (4), 243-257.

Cording E.J. and Hansmire W.H. (1975). "Displacement around soft tunnels". *Proc. 5<sup>th</sup>*



Pam-Am Conf. on Soil Mech. and Found. Engineering, Buenos Aires, Vol. 4, pp. 571-633.

Divall S. and Goodey R.J. (2012). Novel apparatus for generating ground movements around sequential twin tunnels in over-consolidated clay. Online publication by Proceedings of the ICE: Geotechnical Engineering, 10-11.

Divall S. (2013). Ground Movements Associated with Twin-tunnel Construction in Clay. PhD thesis, City University London, London, UK.

Divall, S. and Goodey, R.J. (2015). Twin-tunnelling-induced ground movements in clay. Proceedings of the Institution of Civil Engineers: Geotechnical Engineering, 168(3), pp. 247-256.

Fargnoli, V., Boldini, D., Amorosi, A., 2015. Twin tunnel excavation in coarse grained soils: observations and numerical back-predictions under free field conditions and in presence of a surface structure. Tunnelling and Underground Space Technology 49, 454-469.

Grant, R.J. (1998). Movements around a tunnel in two-layer ground. Ph.D. Thesis, City University London.

Hunt D.V.L. (2005). Predicting the ground movements above twin tunnels constructed in london clay. PhD thesis, University of Birmingham, Birmingham, UK.

Kim S. H., Burd H. J., and Milligan G.W.E. (1998). Model testing of closely spaced

tunnels in clay. *Géotechnique*. 48(48):375–88.

Lee C.J., Wu B.R., Chen H.T., Chiang K.H. (2006). Tunnel stability and arching effects during tunneling in soft clayey soil. *Tunnelling and Underground Space Technology*. 21: 119-32.

Mair, R.J. (1979). Centrifugal modelling of tunnel construction in soft clay. PhD thesis, University of Cambridge, Cambridge, UK.

Masin D. (2004). Laboratory and Numerical Modelling of Natural Clays. MPhil thesis, City University, London, UK.

Morrison, P. R. J. (1994). Performance of foundations in a rising groundwater environment. PhD thesis, City University, London, UK.

Nyren R. (1998). Field Measurements Above Twin Tunnels in London Clay. PhD thesis, Imperial College London, UK.

O'Reilly M.P. and New B.M., (1982). Settlements above tunnels in the United Kingdom - their magnitude and prediction, *Tunnelling' 82*, Papers presented at the 3<sup>rd</sup> International Symposium, Inst of Mining and Metallurgy, London, England, pp. 173-181.

Peck, R.B. Deep excavations and tunnelling in soft ground. *Proc. 7<sup>th</sup> ICSMFE*. 1969; 225–90.

Roscoe K.H. and Burland J.B. (1968). On the generalised stress–strain behaviour of a

- ‘wet’ clay, in engineering plasticity. In: Heyman, Leckie, editors, pp. 535–609.
- Schofield A.N. (1980). Cambridge geotechnical centrifuge operations. *Géotechnique*. 30(3):227–68.
- Stallebrass S. E. (1990). The effect of recent stress history on the deformation of overconsolidated soils. PhD thesis, City University, London, UK.
- Stallebrass S.E. and Taylor R.N. (1997). The development and evaluation of a constitutive model for the prediction of ground movements in overconsolidated clay. *Géotechnique*. 47(2):235–53.
- Taylor R.N. (1984). Ground movements associated with tunnels and trenches. PhD thesis, University of Cambridge, Cambridge, UK.
- Viggiani, G. (1992). Small strain shear stiffness of fine grained soils. PhD thesis, City University, London, UK.